Clim. Past Discuss., 11, 27–61, 2015
www.clim-past-discuss.net/11/27/2015/
doi:10.5194/cpd-11-27-2015

Climate of the Past
Discussions
Open Access

How might the North American ice sheet influence the Northwestern Eurasian climate?

P. Beghin[1], **S. Charbit**[1], **M. Kageyama**[1], **C. Dumas**[1], **and C. Ritz**[2]

[1]Laboratoire des Sciences du Climat et de l'Environnement, CEA-CNRS, Gif-sur-Yvette, France
[2]Laboratoire de Glaciologie et de Géophysique de l'Environnement, CNRS, Saint Martin d'Hérès, France

Received: 8 December 2014 – Accepted: 11 December 2014 – Published: 7 January 2015

Correspondence to: P. Beghin (pauline.beghin@lsce.ipsl.fr)

Published by Copernicus Publications on behalf of the European Geosciences Union.

Abstract

During the last glacial period (∼ 21 000 years ago), two continental-scale ice sheets covered the Canada and northern Europe. It is now widely acknowledged that these past ice sheets exerted a strong influence on climate by causing changes in atmospheric and oceanic circulations. In turn, these changes may have impacted the development of the ice sheets themselves through a combination of different feedback mechanisms. The present study is designed to investigate the potential impact of the North American ice sheet on the surface mass balance (SMB) of the Eurasian ice sheet through simulated changes in the past glacial atmospheric circulation. Using the LMDz5 atmospheric circulation model, we carried out twelve experiments run under constant Last Glacial Maximum (LGM) conditions for insolation, greenhouse gases and ocean. In the all experiments, the Eurasian ice sheet is removed. The twelve experiments differ in the North American ice-sheet topography, ranging from a white and flat (present-day topography) ice sheet to a full-size LGM ice sheet. This experimental design allows to disentangle the albedo and the topographic impacts of the North American ice sheet onto the climate. The results are compared to our baseline experiment where both the North American and the Eurasian ice sheets have been removed. In summer, we show that the only albedo effect of the American ice sheet modifies the pattern of planetary waves with respect to the no-ice sheet case, causing a cooling of the Eurasian region. By contrast, the atmospheric circulation changes induced by the topography of the North American ice sheet imply summer warming in Northwestern Eurasia. In winter, the Scandinavian and the Barents–Kara regions respond differently to the albedo effect: in response to atmospheric circulation changes, Scandinavia is warmed up and precipitation is more abundant whereas Barents–Kara area is cooled down, decreasing convection process and thus leading to less precipitation. The height increase of American ice sheet leads to less precipitation and snowfalls and colder temperatures over both Scandinavian and Barents–Kara sectors. The simulated temperature and precipitation fields have then been used to force an ice-sheet model

and to compute the resulting surface mass balance over the Fennoscandian region as a function of the American ice-sheet configuration. It clearly appears that the SMB is dominated by the ablation signal. In response to the summer cooling induced by the American ice-sheet albedo, a highly positive SMB is simulated over the Eurasian ice sheet, leading thus to the growth of the ice sheet. On the contrary, the topography of the American ice sheet leads to more ablation, hence limiting its growth.

1 Introduction

The last million years is characterized by alternating glacial and interglacial phases. During glacial periods, large ice sheets covering present-day Canada and northwestern Eurasia (Peltier, 2004; Lambeck et al., 2006; Tarasov et al., 2012; Clark et al., 1993; Dyke and Prest, 1987; Svendsen et al., 2004) exerted a strong influence on climate. Several studies highlighted the importance the climatic changes induced by continental-scale ice sheets (Clark, 1999). It has been recognized that the ice-sheet topography is likely to be the main factor altering the atmospheric circulation in the Northern Hemisphere (Broccoli and Manabe, 1987; Pausata et al., 2011). As an example, the pioneering study carried out by Manabe and Broccoli (1985) with an atmospheric general circulation model (AGCM) shows that the North American ice sheet caused a split of the westerlies. The authors also highlight a larger amplitude of the planetary waves due to the presence of ice sheets. Recently, Ullman et al. (2014) tested the influence of different North American ice-sheet reconstructions on the climate. They showed that a higher American ice sheet leads to a more zonal Atlantic jet, and therefore confirmed the key role of ice-sheet topography on atmospheric circulation. Using model outputs from the Past Model Intercomparison Project 2 (PMIP2) Braconnot et al. (2007); Laîné et al. (2008) and Rivière et al. (2010) highlight a strengthening and an equatorward displacement of the sub-tropical jet-stream during the Last Glacial Maximum (LGM) w.r.t. pre-industrial (PI) period. Changes in the position and the strength of the North Atlantic jet stream induce changes in the storm tracks, and therefore in precipitation (Kageyama and Valdes, 2000; Hall et al., 1996; Laîné et al., 2008; Rivière et al., 2010). These changes have also an influence on the energy transport and therefore modify the temperature.

The climatic changes induced by large-scale ice sheets exert an influence on both temperature and precipitation that drive the ice-sheet surface mass balance, defined as the sum of snow accumulation and ablation. Using a simple ice-sheet model based on an idealized geometry coupled to a stationary-wave model, Roe and Lindzen (2001a, b) highlight the importance of accounting for the feedbacks between ice sheets and temperatures induced by changes in stationary waves to properly simulate the evolution of an ice sheet. They show that the self-induced temperature anomaly due to an ice sheet leads to a warming over the ice-sheet western part. This may explain the absence of ice over Alaska at the LGM. They also suggest that the stationary waves excited by the North American ice sheet ice sheet may have contributed to a warming over Europe, influencing the development of the Eurasian ice sheet. In the same way, with a three-dimensional stationary wave model, Liakka et al. (2011) showed that the southern margin of ice sheets strongly depends on the temperature anomalies due to stationary waves, which are modified by the ice-sheet itself. More recently, with the use of the CAM3 atmospheric model run under four different climatic contexts (last interglacial, MIS5b, MIS4, and LGM periods), Löfverström et al. (2014) show how the atmospheric circulation changes induced by the ice sheets could have influenced the growth of the ice sheets themselves. Like Roe and Lindzen (2001b), they show that the summer atmospheric circulation change due to the presence of ice sheets may cause a sufficient warming over Siberia and Alaska to inhibit ice growth. They also perform two experiments under MIS4 conditions to test the influence of one ice sheet on the other one. They conclude that the summer temperature anomaly due to the presence of the MIS4 American ice sheet is too weak to explain the small size of the European ice sheet at that period, but may have contributed to the westward shift of the ice-sheet mass center. Although several studies have been devoted to the influence of one ice sheet on the other one (Roe and Lindzen, 2001b; Beghin et al., 2014; Löfverström et al., 2014), no study has specifically investigated the mechanisms through which the American ice sheet may have influenced the European climate, and therefore the European ice-sheet surface mass balance.

The aim of this paper is to investigate the American ice sheet albedo and topography effects on the Scandinavian and Barents–Kara climates. To achieve this goal, we use the LMDz5 atmospheric general circulation model run with different thicknesses of the North American ice sheet taken as boundary conditions, with no ice at all over Eurasia. We investigate the mechanisms by which the American ice sheet may change the surface mass balance of the Eurasian ice sheet. Finally, we use climatic fields simulated by the LMDz5 model as inputs to a three-dimensional ice-sheet model to compute the surface mass balance of the European ice sheet. The description of the climate and ice-sheet models are made in Sect. 2 as well as the experimental design. The model results are presented in both Sects. 3 and 4. Section 5 summarizes the main findings of our study.

2 Model and experiment

2.1 The atmospheric model

The atmospheric LMDz5 model used in this study is a climate model developed at Laboratoire de Météorologie Dynamique (Sadourny and Laval, 1984; Le Treut et al., 1994, 1998). LMDz is the atmospheric part of the IPSL-CM5A coupled ocean-atmosphere model. The dynamical equations are discretized on a longitude-latitude-staggered Arakawa C-grid (Kasahara, 1977). The model ensures the conservation of both enstrophy (square of wind rotational) for barotropic flows (Sadourny, 1975a, b) and the axi-symmetric component of the angular momentum. The model version used in this study has 39 vertical levels and runs on a 96 × 95 model grid resolution (3.75° × 1.9°). A complete description of the model can be found in Hourdin et al. (2006).

CPD
11, 27–61, 2015

2.2 The ice-sheet model

The ice-sheet model GRISLI is a three-dimensional thermo-mechanical model which simulates the evolution of ice-sheet geometry (extension and thickness) and the coupled temperature-velocity fields in response to climate forcing. A comprehensive description of the model can be found in Ritz et al. (2001) and Peyaud et al. (2007). Here, we only summarize the main characteristics of this model. The equations are solved on a cartesian grid (40 km × 40 km). Over the grounded part of the ice sheet, the ice flow resulting from internal deformation is governed by the shallow-ice approximation (Morland et al., 1984; Hutter, 1983). The model also deals with ice flow through ice shelves using the shallow-shelf approximation (MacAyeal, 1989). It also predicts the large-scale characteristics of the ice streams using criteria based on the effective pressure and hydraulic load. At each time step, the velocity and vertical profiles of temperature in the ice are computed as well as the new geometry of the ice sheet. The isostatic adjustment of bedrock in response to ice load is governed by the flow of the asthenosphere, with a characteristic time constant of 3000 years, and by the rigidity of the lithosphere. The temperature field is computed both in the ice and in the bedrock by solving a time-dependent heat equation. The surface mass balance is defined as the sum between accumulation and ablation computed by the empirical positive degree day (PDD) method (Reeh, 1991; Fausto et al., 2009). This method assumes that melt rates of snow and ice are linearly related to the number of PDD through degree-day factors for snow and ice materials (Braithwaite, 1984, 1995).

2.3 Experimental set-up

In order to investigate the albedo and topography effects induced by the North American ice sheet on the Eurasian climate at the LGM, we carried out 12 simulations under LGM conditions (GHG, insolation, sea-surface temperatures and sea-ice). In this series of simulation, the altitude of the North American ice sheet surface ranges from that of the present-day surface to 100 % of that used in the PMIP3 LGM experiments.

CPD
11, 27–61, 2015

The PMIP3 LGM ice sheets result from a combination of three reconstructions, namely ICE-6G v2.0 (Peltier, 2009), GLAC-1 (Tarasov et al., 2012) and ANU (Lambeck, 2001). The way this new reconstruction has been obtained is explained in detail on the PMIP3 website (http://pmip3.lsce.ipsl.fr). In our baseline experiment (noIS), the land-ice mask is modified (w.r.t. PMIP3) to remove both the European ice sheet and the American ice sheet (Fig. 1). In the other simulations, we only removed the European ice-sheet mask. These simulations are referred to as *xx* dhL, where dhL represents the surface height difference between the PMIP3 LGM ice sheet and the present-day surface, and *xx* represents the percentage of dh taken into account. Note that to simplify the writing, the all American and all Eurasian ice sheets are respectively referred to as the "Laurentide ice sheet" (LIS) and the "Fennoscandian ice sheet" (FIS) in all figures and in the following text.

The topography of the 00 dhL experiment is therefore the same as today, but the land-ice mask is set to the LGM one (Fig. 2). Greenland and Antarctica ice sheets are the same as in the PMIP3 experimental set-up. Both insolation and GHG boundary conditions are similar to those defined in the PMIP3 protocol: the orbital forcing is taken at 21 kyr BP from Berger et al. (1998), while atmospheric greenhouse gas concentrations are those recorded in Antarctic ice cores (CO_2 = 185 ppm, (Lüthi et al., 2008); CH_4 = 350 ppb, (Loulergue et al., 2008); N_2O = 200 ppb, (Spahni, 2005)). The LGM land-sea mask is also taken into account, with closed Bering Strait, and land in Hudson Bay and Barents Sea (Fig. 1). The sea-surface temperatures (SST) and the sea-ice come from the IPSL PMIP3 LGM run outputs (Kageyama et al., 2013), and have therefore an interannual variability. The simulations are run for 60 years, and we study the last 40 years to be at equilibrium.

3 AGCM results

In this section, we focus on how the LIS influences the climatic fields having an impact on the surface mass balance of an ice sheet. If we use the PDD method to compute ablation, the key climatic variables are therefore the monthly temperatures and the monthly total (solid and liquid) precipitation.

3.1 Impact of the LIS on temperature

We first consider the LIS albedo effect using the comparison between the 00 dhL and the noIS experiment. The LIS albedo effect on the Scandinavian–Barents–Kara (SBK) summer 2 m air temperature leads to a cooling over the whole Eurasian continent (Fig. 3, 00 dhL experiment, left column) with a maximum centered over the Barents–Kara seas (more than −10 °C). This maximum corresponds to the zone where the albedo is the largest (orange contours). This is due to the LGM land-sea mask used in this study: the Barents–Kara seas are represented as land in our simulations, allowing snow accumulation and therefore higher albedo in this area. There is therefore a positive feedback on temperature. Figure 3 also displays the 2 m mean summer temperature over the SBK region for different altitudes of the LIS. Note that we only give results of selected experiments to simplify the presentation of our results. Figure 3 clearly shows that the SBK cooling gets smaller when the LIS gets higher. When the LIS reaches its full LGM size (100 dhL-noIS), the cooling over Barents–Kara seas reaches 4–6 °C. The topography of the LIS has therefore a warming effect on the SBK region.

In winter, (Fig. 3 right panels), the LIS albedo induces warmer temperatures (+3 °C) over Scandinavia and the British Isles, and cooler temperatures over Barents–Kara (−3 °C). In the 60 dhL experiment, the cooling spreads across the entire Scandinavia–Barents–Kara area, and the cooling is stronger when the LIS is higher. The LIS topography therefore leads to colder winter temperatures over the Scandinavia–Barents–Kara area.

To understand the origin of these contrasted responses, we investigate through which processes the changes in the altitude of the Laurentide ice sheet modify the atmospheric circulation.

CPD
11, 27–61, 2015

3.2 Atmospheric circulation

The comparison of the 500 hPa summer geopotential height zonal anomaly between noLIS and 00 dhL shows that the sole albedo effect of the LIS is sufficient to drastically change the atmospheric circulation (Fig. 4, 00 dhL, left column). The ridge over the Rockies, clearly visible in noLIS, has disappeared in 00 dhL, and the trough over the Labrador sector is more expanded. Ridges over the North Atlantic, the Greenland ice sheet and northern Europe are more developed in 00 dhL (w.r.t. noIS). By contrast the troughs over Iceland, the Norvegian and Barents seas in noIS are weaker or even vanished in 00 dhL. In noIS, the trough over Svalbard implies southerlies over the Barents sea (Fig. 4, right column), and therefore warm temperatures in this area (Fig. 3). The weakening of this trough in 00 dhL as well as the stronger ridge over Greenland induces northerlies over Svalbard and the Barents sea (Fig. 4), and therefore colder temperatures (Fig. 3).

The Labrador trough and the North Atlantic ridge become stronger when the LIS gets higher, until it reaches 60 % of its full size. Beyond 60 dhL, the Labrador trough and the Atlantic ridge keep more or less the same amplitude. When the LIS gets higher, the Greenland ridge gets weaker, the European ridge remains more or less the same (Fig. 4), and there is a return of the Iceland–Svalbard–Barents trough. This new trough, centered between Greenland and Svalbard, along with the weakening of the Greenland ridge, brings southerlies again over the northern Barents sea. The Barents winds shift from northerlies to southerlies when the LIS is 60 % of its full size. The southerlies bring warmer temperatures, explaining the decrease of the SBK cooling with the increase of the LIS height (Figs. 3 and 4).

In winter (Fig. 5), the sole albedo effect of the LIS does not drastically change the geopotential anomaly. However, the meridional wind field shows a slight decrease of the southerlies over the Barents sea, explaining the cooling over this region. One can also observe a slight decrease of the northerlies over the British Isles, Europe and southern Scandinavia, consistent with the slight warming simulated over this region.

CPD
11, 27–61, 2015

A higher LIS implies the emergence of a trough over the Scandinavian–Barents sector. This trough comes with northerlies over the Norvegian sea and weaker southerlies over the Barents sea (Fig. 5, right column), consistently with colder temperatures over this area, as seen in Fig. 3.

This analysis explains why opposite temperature reponses are obtained in both summer and winter seasons. Since ablation is rather sensitive to the summer season, more ice is expected over the Fennoscandian area when the sole albedo effect of the LIS is operating (i.e. 00 dhL experiment). The development of an ice sheet in this area also crudely depends on snow accumulation. Therefore, we examine hereafter the LIS impact on the SBK precipitation and snowfall.

3.3 Impact of the LIS on northwestern Eurasian precipitation and snowfall

In this section, we investigate the impact of the LIS on the northwestern Eurasian annual precipitation and snowfall. Figure 6 shows that the sole albedo effect (00 dhL-noIS panel) induces more precipitation over the northern British Isles and Scandinavia, but less precipitation over the Barents–Kara area. However, over the whole SBK region, the snowfall anomaly is positive due to a negative temperature anomaly (see Fig. 3) allowing to increase the fraction of solid precipitation and to maintain the snow cover.

When the LIS becomes higher, the positive anomaly of precipitation over Scandinavia simulated in the 00 dhL experiment shifts southward, even reaching the French and the Iberian Peninsula Atlantic coasts as the LIS reaches its LGM altitude (100 dhL-noIS). Concomitantly, the negative anomaly of precipitation over the Barents–Kara region in 00 dhL expands westward leading to a dryer climate and to a decrease of snowfall. These results suggest that the Barents–Kara and the Scandinavian region are sensitive to different characteristics of the LIS: whereas the precipitation over Scandinavia appears to be sensitive to the LIS height, the precipitation anomaly over the Barents–Kara regions seems to mainly result from the albedo effect of the LIS and is rather insensitive to height.

CPD
11, 27–61, 2015

To disentangle the mechanisms responsible for precipitation changes in these regions we split up the precipitation into its large-scale and convective components (Fig. 7). In the large-scale component (Fig. 7, left panels), the positive anomaly of precipitation simulated over the British Isles and over Scandinavia in 00 dhL, and the southward shift of this pattern simulated when the LIS gets higher are also found. In the same way, drier Scandinavian conditions with the full-LGM LIS (100 dhL-noIS) are still present. This strongly suggests that the Scandinavian precipitation, as expected, is driven by large-scale processes.

The negative anomaly of precipitation appearing in the Arctic Ocean north of the Barents–Kara area is also found in the large-scale component, but the large negative precipitation anomaly south of the Novaya Zemlya clearly comes from convective processes. The decrease of the convective precipitation negative anomaly when the LIS is higher can be easily explained by the decrease of the negative anomaly of summer temperatures mentioned above.

To further investigate the mechanisms governing precipitation over the Scandinavian and Barents–Kara regions, we first examine the seasonality of precipitation. To achieve this goal, we compute the average precipitation above Scandinavia (55–70° N : 0–20° E) (Fig. 8a) and the Barents–Kara region (65–90° N : 20–100° E) (Fig. 8b), and we compare summer and winter precipitation anomalies with the annual precipitation anomaly. This shows that winter precipitation changes are clearly correlated with annual precipitation ($r = 0.99$) over Scandinavia. This means that the annual signature observed over Scandinavia (Figs. 6 and 7) is mainly due to winter precipitation. By contrast, the Barents–Kara sector is linked to the summer precipitation, at least for LIS sizes up to 60 % of the full LGM size (Fig. 8b).

3.4 Precipitation changes over Scandinavia: implication of the jet stream shift

We therefore look for a winter mechanism explaining Scandinavian precipitation. Using PMIP3 model outputs for the LGM, Beghin et al. (2015, submitted) found a correlation between the southward shift of the North Atlantic jet stream between PI and LGM runs and the winter precipitation over the Iberian Peninsula. Following the same approach, we examine whether a mechanism similar to the one found in Beghin et al. (2015, submitted) may explain the precipitation changes over Scandinavia in case of changes in LIS characteristics.

Similarly to Chavaillaz et al. (2013), we use the 850 hPa zonal wind to define the jet stream. The position of the jet displayed in Fig. 9 corresponds to the position of the 850 hPa meridional wind maximum. The LIS albedo effect induces a slight northward shift of the North Atlantic jet stream (00 dhL-noIS pannel). As the LIS becomes higher, the jet goes progressively southward and shifts southward of its noIS position between 30 and 50 dhL. In these experiments, the Scandinavian winter precipitation anomaly becomes negative. This suggests a relationship between the shift of the North Atlantic jet stream and the precipitation over the Scandinavian region.

To confirm this assumption, we plot the shift of the jet ($\Delta\phi$) as a function of the precipitation difference between the noIS and the xx dhL experiments over Scandinavia (Fig. 10). $\Delta\phi$ is defined as the difference of latitudes between noIS and xx dhL experiments where the 850 hPa zonal wind is maximum. The latitude of this maximum has been found by computing the zonal mean of the zonal wind over the Atlantic basin (50–10° W) and then by extrapolating the maximum by regression. This method allows to find the exact latitude of the jet maximum (Chavaillaz et al., 2013; Beghin et al., 2015, submitted). We find a good correlation between the shift of the North Atlantic jet and the Scandinavian precipitation anomaly during the winter season (Fig. 10). The quantification of the range of the precipitation anomalies and of the jet shift is obtained by bootstrapping: a sample of thousand values is obtained by calculating the average of 1000 randomly picked samples of 40 year-duration in the noIS and the xx dhL original samples. Linear regressions of the 5th and 95th percentiles of the bootstrapping sample confirm the close link between the shift of the North Atlantic jet stream and the winter precipitation changes over Scandinavia due to the effect of LIS.

The 500 hPa geopotential zonal anomaly (Fig. 5) shows a slight southward expansion of the Labrador trough as the LIS gets higher. Figure 11 shows that the expansion of the Labrador trough as the LIS gets higher pushes the westerlies southward. Moreover, the strengthening of the European trough pushes the westerlies southward over the eastern Atlantic (Fig. 5). These two effects explain the southward shift of the North Atlantic jet stream when altitude of the LIS increases.

3.5 Precipitation changes over Barents–Kara area

The comparison of the annual (Fig. 6), summer and winter (Fig. 9) precipitation anomalies over Barents–Kara, and more specifically, the comparison of seasonal precipitation (Fig. 8b) suggests that the summer response dominates the annual signal when the LIS remains at a relatively low level (60 % of PMIP3 LIS height). The total amount of summer precipitation is lower when the only LIS albedo effect is accounted for (i.e. 00 dhL w.r.t. noIS experiment), but the snowfall anomaly is positive (more than $+0.5\,\mathrm{mm\,day^{-1}}$). When the LIS becomes higher, the summer precipitation anomaly is less negative, probably due to more convective precipitation resulting from warmer temperatures (Fig. 3).

To summarize, the LIS albedo effect induces colder summer temperatures over the northwestern Eurasia (SBK area) w.r.t. the noIS experiment, and more precipitation over Scandinavia and the British Isles due to a northward shift of the winter jet. It also induces less precipitation over the Barents–Kara area due to colder temperatures, and therefore less convective precipitation. The snowfall amount over the Barents–Kara region is however larger with a flat and white LIS, due to colder temperatures. Over Scandinavia, the winter temperatures are warmer, due to weaker northerlies and to the poleward shift of the Atlantic jet stream.

The higher the LIS, the weaker the negative anomaly of summer temperature over Barents–Kara, due to changes in the atmospheric circulation. The higher the LIS, the smaller the amounts of annual precipitation and snowfall over the Scandinavian and the Barents–Kara areas, in response to the equatorward shift of the jet.

CPD
11, 27–61, 2015

4 Analysis of ice-sheet model outputs: consequences on the surface mass balance

To go a step further, we investigate the impact of the LIS on the surface mass balance of both Scandinavian and Barents-KAra areas. To do this, we use the LMDz5 monthly temperatures and precipitation fields of each experiment to force the ice-sheet model GRISLI. LMDz5 climatic fields are downscaled over the GRISLI grid using a bilinear interpolation. Due to the difference of resolution between the atmospheric and the ice-sheet models, temperature is vertically corrected using a linear vertical gradient of $6\,^{\circ}\mathrm{K\,km^{-1}}$. Precipitation is also vertically corrected using an exponential function of the temperature (Charbit et al., 2002, 2007). Snowfall is recalculated using the downscaled precipitation and temperature because the more detailed topography seen by GRISLI allows snowfall when LMDz5 provides only liquid precipitation.

Figure 12 displays the snow accumulation and the ablation fields computed by GRISLI for the five selected experiments. As expected from the LMDz5 results of annual precipitation and snowfall, snow accumulation over Scandinavia is larger when the LIS is flat and decreases as the LIS is higher. A similar observation can be made over the Barents–Kara region. Consistently with the simulated summer temperatures, when the LIS is flat, the ablation is weaker over the entire SBK region, and increases as the LIS gets higher. Neverthless, even with the full-LGM LIS, the ablation remains weaker than in the noIS experiment.

The resulting surface mass balance is shown in Fig. 13a. The similarities between the ablation (Fig. 12b) and the surface mass balance patterns indicate that the surface mass balance is dominated by the ablation. In the absence of LIS, the surface mass balance is positive over only a small part of the SBK area, that is over the Svalbard. Under these conditions, no ice sheet can therefore grows (Fig. 13b). When the LIS is flat, the surface mass balance is positive over the Barents–Kara seas and over the northern part of Scandinavia, allowing the growth of ice. Note that the simulated FIS is less extended than those provided by the ICE-6G (Peltier, 2009) and the ANU

CPD
11, 27–61, 2015

(Lambeck, 2001) reconstructions. This is likely due to the absence of albedo feedback, since our approach is only based on a one-way coupling. As the LIS gets higher, the limit of the positive surface mass balance shifts westward and northward, excluding the Kara sea and Scandinavia from the positive surface-mass balance area. When the LIS has its full LGM size, the surface mass balance is positive only over the Svalbard. As a consequence, the simulated FIS is smaller.

5 Discussion

Geomorphological reconstructions revealed that the Fennoscandian ice sheet eastern limit reached the Putorana Mountains in Siberia during the Early Weichselian (90–80 kyr BP) (Svendsen et al., 2004; Mangerud et al., 1998). According to Svendsen et al. (2004), this eastern limit moved back to the Kara sea around 60 kyr BP, along with the southward extension of the Scandinavian ice sheet (Mangerud et al., 1998; Andersen and Mangerud, 1989; Lundqvist, 1992; Houmark-Nielsen, 1999). At the LGM, the ice sheet finally reached the British Isles, and the Kara ice shelf did not cover the entire Kara sea anymore (Svendsen et al., 2004; Landvik et al., 1998; Ehlers et al., 2004). The recent study of Kleman et al. (2013) shows that the FIS reached its maximum ice volume at 60 kyr BP.

Löfverström et al. (2014) propose to attribute the westward shift of the FIS and the decrease of the Kara ice sheet to warmer temperatures over Siberia induced by the LIS, along with the upslope precipitation effect proposed by Sanberg and Oerlemans (1983).

Contrary to Löfverström et al. (2014), our simulations used non-realistic LIS geometry, and are therefore idealized experiments. The advantage of our experimental setup is that the impact of the LIS albedo and topography can be studied separately. Our study clearly shows that the LIS impact on the FIS depends on its topography. Within a glaciation context, a large but low LIS will favor a positive SMB over the SBK sector, and therefore the FIS maintenance. By contrast, as the LIS gets higher, ablation increases leading to a smaller FIS. Our results therefore suggest that the LIS growth after 60 kyr BP may have contributed to progressively slow down the FIS growth and finally to trigger the westward retreat of the ice sheet, which is in agreement with findings of Kleman et al. (2013). These results could also suggest that the larger size of the FIS during the late Saalian (around 140 ka) w.r.t. the LGM was due to a smaller LIS.

6 Conclusions

The goal of this study was to investigate the atmospheric processes through which the LIS can influence the northwestern Eurasian climate, and therefore how it can influence the FIS surface mass balance. We performed twelve simulations under LGM conditions, but with different ice-sheet configurations. In our baseline experiment, the LIS and the FIS are removed. In the other simulations, we only removed the FIS, and the LIS has different heights. We therefore identified the effect of the LIS albedo and topography on the northwestern European climate. We focus on the fields having an impact on ice-sheet surface mass balance, i.e. the temperature and the precipitation. We show that:

1. The LIS albedo decreases the summer temperatures over the Fennoscandian sector. This decrease is amplified by positive snow albedo feedback. This positive feedback is somewhat related to our experimental setup, which includes land over Barents–Kara instead of water, allowing snow maintenance. The temperature decrease is weaker when the LIS is higher, due to atmospheric circulation changes.

2. In winter, the LIS albedo impact decreases the Barents–Kara temperature, but increases the Scandinavian temperature. The higher the LIS, the colder the temperature over the whole Fennoscandian sector.

CPD
11, 27–61, 2015

3. The effect of LIS albedo also tends to shift poleward the North Atlantic jet stream, and to bring more precipitation and snowfall over Scandinavia. When the LIS is higher, the Atlantic jet shifts equatorward, bringing less precipitation over northern Europe. As a consequence, precipitation and snowfall decrease over Scandinavia and Barents–Kara sectors when the LIS is higher.

We used the LMDz5 precipitation and temperature fields to force the ice-sheet model GRISLI. We therefore took a look on the LIS impact on ablation, accumulation, and ice-sheet shape. The GRISLI simulations show that the presence of the LIS albedo favors the growth of the FIS, essentially because of weak ablation. As the LIS gets higher, the FIS is smaller due to more ablation, in accordance with the LMDz5 summer temperature conclusions. When the LIS reaches its full-LGM size, there is ice only over the Svalbard.

This study highlights the mechanisms by which the LIS can influence the FIS surface mass balance. The use of the ice-sheet model allows to illustrate the impact of climatic changes due to the LIS presence on the FIS. It shows that the albedo of the LIS favors the FIS growth whereas the LIS topography acts against the FIS growth. Even if this study does not simulate a transient glaciation, it gives clues about the relation the two ice sheets may have had during their build-up. The ablation increase over Barents–Kara seas when the LIS has its LGM size may have contribute to the LGM FIS small size.

References

Andersen, B. G. and Mangerud, J.: The last interglacial-glacial cycle in Fennoscandia, Quatern. Int., 3, 21–29, 1989. 41

Beghin, P., Charbit, S., Dumas, C., Kageyama, M., Roche, D. M., and Ritz, C.: Interdependence of the growth of the Northern Hemisphere ice sheets during the last glaciation: the role of atmospheric circulation, Clim. Past, 10, 345–358, doi:10.5194/cp-10-345-2014, 2014. 30

Beghin, P., Charbit, S., Kageyama, M., Combourieu-Nebout, N., Hatte, C., Dumas, C., and Peterschmitt, J.: What drives LGM precipitation over the Western Mediterranean?, Clim. Dynam., under review, 2015. 37, 38

Berger, A., Loutre, M. F., and Gallée, H.: Sensitivity of the LLN climate model to the astronomical and CO_2 forcings over the last 200 ky, Clim. Dynam., 14, 615–629, doi:10.1007/s003820050245, 1998. 33

Braconnot, P., Otto-Bliesner, B., Harrison, S., Joussaume, S., Peterchmitt, J.-Y., Abe-Ouchi, A., Crucifix, M., Driesschaert, E., Fichefet, Th., Hewitt, C. D., Kageyama, M., Kitoh, A., Laîné, A., Loutre, M.-F., Marti, O., Merkel, U., Ramstein, G., Valdes, P., Weber, S. L., Yu, Y., and Zhao, Y.: Results of PMIP2 coupled simulations of the Mid-Holocene and Last Glacial Maximum – Part 1: experiments and large-scale features, Clim. Past, 3, 261–277, doi:10.5194/cp-3-261-2007, 2007. 29

Braithwaite, R.: Calculation of degree-days for glacier-climatic research, Zeitschrift für Gletscherkunde und Glazialgeologie, 20, 1–18, 1984. 32

Braithwaite, R. J.: Positive degree-day factors for ablation on the Greenland ice sheet studied by energy-balance modelling, J. Glaciol., 41, 153–160, 1995. 32

Broccoli, A. and Manabe, S.: The influence of continental ice, atmospheric CO_2, and land albedo on the climate of the Last Glacial Maximum, Clim. Dynam., 1, 87–99, 1987. 29

Charbit, S., Ritz, C., and Ramstein, G.: Simulations of Northern Hemisphere ice-sheet retreat: sensitivity to physical mechanisms involved during the Last Deglaciation, Quaternary Sci. Rev., 21, 243–265, 2002. 40

Charbit, S., Ritz, C., Philippon, G., Peyaud, V., and Kageyama, M.: Numerical reconstructions of the Northern Hemisphere ice sheets through the last glacial-interglacial cycle, Clim. Past, 3, 15–37, doi:10.5194/cp-3-15-2007, 2007. 40

Chavaillaz, Y., Codron, F., and Kageyama, M.: Southern westerlies in LGM and future (RCP4.5) climates, Clim. Past, 9, 517–524, doi:10.5194/cp-9-517-2013, 2013. 38

Clark, P. U.: Northern Hemisphere ice-sheet influences on global climate change, Science, 286, 1104–1111, doi:10.1126/science.286.5442.1104, 1999. 29

Clark, P., Clague, J., Curry, B., Dreimanis, A., Hicock, S., Miller, G., Berger, G., Eyles, N., Lamothe, M., Miller, B., Mott, R., Oldale, R., Stea, R., Szabo, J., Thorleifson, L., and Vincent, J.-S.: Initiation and development of the Laurentide and Cordilleran Ice Sheets following the last interglaciation, Quaternary Sci. Rev., 12, 79–114, doi:10.1016/0277-3791(93)90011-A, 1993. 29

CPD
11, 27–61, 2015

North American ice sheet influence on the Eurasian climate

P. Beghin et al.

Dyke, A. S. and Prest, V. K.: Late Wisconsinan and Holocene history of the Laurentide Ice Sheet, Geogr. Phys. Quatern., 41, 237, doi:10.7202/032681ar, 1987. 29

Ehlers, J., Eissmann, L., Lippstreu, L., Stephan, H.-J., and Wansa, S.: Pleistocene glaciations of north Germany, Develop. Quat. Sci., 2, 135–146, 2004. 41

Fausto, R. S., Ahlström, A. P., van As, D., Johnsen, S. J., Langen, P. L., and Steffen, K.: Improving surface boundary conditions with focus on coupling snow densification and meltwater retention in large-scale ice-sheet models of Greenland, J. Glaciol., 55, 869–878, doi:10.3189/002214309790152537, 2009. 32

Hall, N. M. J., Valdes, P. J., and Dong, B.: The Maintenance of the Last Great Ice Sheets: a UGAMP GCM Study, J. Climate, 9, 1004–1019, doi:10.1175/1520-0442(1996)009<1004:TMOTLG>2.0.CO;2, 1996. 30

Houmark-Nielsen, M.: A lithostratigraphy of Weichselian glacial and interstadial deposits in Denmark, B. Geol. Soc. Denmark, 46, 101–114, 1999. 41

Hourdin, F., Musat, I., Bony, S., Braconnot, P., Codron, F., Dufresne, J.-L., Fairhead, L., Filiberti, M.-A., Friedlingstein, P., Grandpeix, J.-Y. et al.: The LMDZ4 general circulation model: climate performance and sensitivity to parametrized physics with emphasis on tropical convection, Clim. Dynam., 27, 787–813, 2006. 31

Hutter, K.: Theoretical Glaciology: Material Science of Ice and the Mechanics of Glaciers and Ice Sheets, edited by: Reidel, Terra Scientific Pub. Co. , sold and distributed in the USA and Canada by Kluwer Academic Publishers, Dordrecht, Boston, Tokyo, Japan, Hingham, MA, 1983. 32

Kageyama, M. and Valdes, P. J.: Impact of the North American ice-sheet orography on the Last Glacial Maximum eddies and snowfall, Geophys. Res. Lett., 27, 1515–1518, 2000. 30

Kageyama, M., Braconnot, P., Bopp, L., Caubel, A., Foujols, M.-A., Guilyardi, E., Khodri, M., Lloyd, J., Lombard, F., Mariotti, V., Marti, O., Roy, T., and Woillez, M.-N.: Mid-Holocene and Last Glacial Maximum climate simulations with the IPSL model-part I: comparing IPSL-CM5A to IPSL-CM4, Clim. Dynam., 40, 2447–2468, doi:10.1007/s00382-012-1488-8, 2013. 33

Kasahara, A.: Computational aspects of numerical models for weather prediction and climate simulation, in: General Circulation Models of the Atmosphere, (A 78-10662 01-47), Academic Press, Inc., New York, 1–66, 1977. 31

Kleman, J., Fastook, J., Ebert, K., Nilsson, J., and Caballero, R.: Pre-LGM Northern Hemisphere ice sheet topography, Clim. Past, 9, 2365–2378, doi:10.5194/cp-9-2365-2013, 2013. 41, 42

CPD

11, 27–61, 2015

North American ice sheet influence on the Eurasian climate

P. Beghin et al.

Laîné, A., Kageyama, M., Salas-Mélia, D., Voldoire, A., Rivière, G., Ramstein, G., Planton, S., Tyteca, S., and Peterschmitt, J. Y.: Northern Hemisphere storm tracks during the last glacial maximum in the PMIP2 ocean-atmosphere coupled models: energetic study, seasonal cycle, precipitation, Clim. Dynam., 32, 593–614, doi:10.1007/s00382-008-0391-9, 2008. 29, 30

Lambeck, K.: Sea level change through the Last Glacial Cycle, Science, 292, 679–686, doi:10.1126/science.1059549, 2001. 33, 41

Lambeck, K., Purcell, A., Funder, S., Kjaer, K., Larsen, E., and Möller, P.: Constraints on the Late Saalian to early Middle Weichselian ice sheet of Eurasia from field data and rebound modelling, Boreas, 35, 539–575, doi:10.1080/03009480600781875, 2006. 29

Landvik, J. Y., Bondevik, S., Elverhoi, A., Fjeldskaar, W., Mangerud, J., Salvigsen, O., Siegert, M. J., Svendsen, J.-I., and Vorren, T. O.: The last glacial maximum of Svalbard and the Barents Sea area: ice sheet extent and configuration, Quaternary Sci. Rev., 17, 43–75, 1998. 41

Le Treut, H. L., Li, Z., and Forichon, M.: Sensitivity of the LMD general circulation model to greenhouse forcing associated with two different cloud water parameterizations, J. Climate, 7, 1827–1841, 1994. 31

Le Treut, H., Forichon, M., Boucher, O., and Li, Z.-X.: Sulfate aerosol indirect effect and CO_2 greenhouse forcing: equilibriumresponse of the LMD GCM and associated cloud feedbacks, J. Climate, 11, 1673–1684, 1998. 31

Liakka, J., Nilsson, J., and Löfverström, M.: Interactions between stationary waves and ice sheets: linear versus nonlinear atmospheric response, Clim. Dynam., 38, 1249–1262, doi:10.1007/s00382-011-1004-6, 2011. 30

Löfverström, M., Caballero, R., Nilsson, J., and Kleman, J.: Evolution of the large-scale atmospheric circulation in response to changing ice sheets over the last glacial cycle, Clim. Past, 10, 1453–1471, doi:10.5194/cp-10-1453-2014, 2014. 30, 41

Loulergue, L., Schilt, A., Spahni, R., Masson-Delmotte, V., Blunier, T., Lemieux, B., Barnola, J.-M., Raynaud, D., Stocker, T. F., and Chappellaz, J.: Orbital and millennial-scale features of atmospheric CH_4 over the past 800 000 years, Nature, 453, 383–386, doi:10.1038/nature06950, 2008. 33

Lundqvist, J.: Glacial stratigraphy in Sweden, Geol. S. Finl., 15, 43–59, 1992. 41

Lüthi, D., Le Floch, M., Bereiter, B., Blunier, T., Barnola, J.-M., Siegenthaler, U., Raynaud, D., Jouzel, J., Fischer, H., Kawamura, K., and Stocker, T. F.: High-resolution carbon diox-

ide concentration record 650 000–800 000 years before present, Nature, 453, 379–382, doi:10.1038/nature06949, 2008. 33
MacAyeal, D. R.: Large-scale ice flow over a viscous basal sediment: theory and application to ice stream B, Antarctica, J. Geophys. Res.-Sol. Ea., 94, 4071–4087, 1989. 32
Manabe, S. and Broccoli, A. J.: The influence of continental ice sheets on the climate of an ice age, J. Geophys. Res., 90, 2167, doi:10.1029/JD090iD01p02167, 1985. 29
Mangerud, J., Dokken, T., Hebbeln, D., Heggen, B., Ingolfsson, O., Landvik, J. Y., Mejdahl, V., Svendsen, J. I., and Vorren, T. O.: Fluctuations of the Svalbard–Barents Sea Ice Sheet during the last 150 000 years, Quaternary Sci. Rev., 17, 11–42, 1998. 41
Morland, L., Smith, G., and Boulton, G.: Basal sliding relations deduced from ice sheet data, J. Glaciol., 30, 131–139, 1984. 32
Pausata, F. S. R., Li, C., Wettstein, J. J., Kageyama, M., and Nisancioglu, K. H.: The key role of topography in altering North Atlantic atmospheric circulation during the last glacial period, Clim. Past, 7, 1089–1101, doi:10.5194/cp-7-1089-2011, 2011. 29
Peltier, W.: Global glacial isostasy and the surface of the ice-age earth: the ICE-5G (VM2) Model and GRACE, Annu. Rev. Earth Pl. Sc., 32, 111–149, doi:10.1146/annurev.earth.32.082503.144359, 2004. 29
Peltier, W.: Closure of the budget of global sea level rise over the GRACE era: the importance and magnitudes of the required corrections for global glacial isostatic adjustment, Quaternary Sci. Rev., 28, 1658–1674, doi:10.1016/j.quascirev.2009.04.004, 2009. 33, 40
Peyaud, V., Ritz, C., and Krinner, G.: Modelling the Early Weichselian Eurasian Ice Sheets: role of ice shelves and influence of ice-dammed lakes, Clim. Past, 3, 375–386, doi:10.5194/cp-3-375-2007, 2007. 32
Reeh, N.: Parameterization of melt rate and surface temperature on the Greenland ice sheet, Polarforschung, 59, 113–128, 1991. 32
Ritz, C., Rommelaere, V., and Dumas, C.: Modeling the evolution of Antarctic ice sheet over the last 420 000 years: implications for altitude changes in the Vostok region, J. Geophys. Res., 106, 31943–31964, doi:10.1029/2001JD900232, 2001. 32
Rivière, G., Laîné, A., Lapeyre, G., Salas-Mélia, D., and Kageyama, M.: Links between Rossby wave breaking and the North Atlantic Oscillation–Arctic Oscillation in present-day and Last Glacial Maximum climate simulations, J. Climate, 23, 2987–3008, doi:10.1175/2010JCLI3372.1, 2010. 29, 30

CPD
11, 27–61, 2015

Roe, G. H. and Lindzen, R. S.: A one-dimensional model for the interaction between continental-scale ice sheets and atmospheric stationary waves, Clim. Dynam., 17, 479–487, doi:10.1007/s003820000123, 2001a. 30

Roe, G. H. and Lindzen, R. S.: The Mutual Interaction between Continental-Scale Ice Sheets and Atmospheric Stationary Waves, J. Climate, 14, 1450–1465, doi:10.1175/1520-0442(2001)014<1450:TMIBCS>2.0.CO;2, 2001b. 30

Sadourny, R.: Compressible model flows on the sphere, J. Atmos. Sci., 32, 2103–2110, 1975a. 31

Sadourny, R.: The dynamics of finite-difference models of the shallow-water equations, J. Atmos. Sci., 32, 680–689, 1975b. 31

Sadourny, R. and Laval, K.: January and July performance of the LMD general circulation model, New Perspectives in Climate Modeling, 1, 173–197, 1984. 31

Sanberg, J. and Oerlemans, J.: Modelling of pleistocene European ice sheets: the effect of upslope precipitation, Geol. Mijnbouw, 62, 267–273, 1983. 41

Spahni, R.: Atmospheric methane and nitrous oxide of the Late Pleistocene from Antarctic Ice Cores, Science, 310, 1317–1321, doi:10.1126/science.1120132, 2005. 33

Svendsen, J. I., Alexanderson, H., Astakhov, V. I., Demidov, I., Dowdeswell, J. A., Funder, S., Gataullin, V., Henriksen, M., Hjort, C., Houmark-Nielsen, M. et al.: Late Quaternary ice sheet history of northern Eurasia, Quaternary Sci. Rev., 23, 1229–1271, available at: http://linkinghub.elsevier.com/retrieve/pii/S0277379103003421, 2004. 29, 41

Tarasov, L., Dyke, A. S., Neal, R. M., and Peltier, W.: A data-calibrated distribution of deglacial chronologies for the North American ice complex from glaciological modeling, Earth Planet. Sc. Lett., 315–316, 30–40, doi:10.1016/j.epsl.2011.09.010, 2012. 29, 33

Ullman, D. J., LeGrande, A. N., Carlson, A. E., Anslow, F. S., and Licciardi, J. M.: Assessing the impact of Laurentide Ice Sheet topography on glacial climate, Clim. Past, 10, 487–507, doi:10.5194/cp-10-487-2014, 2014. 29

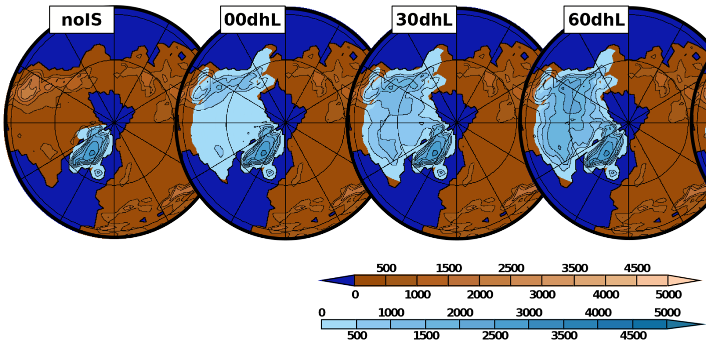

Figure 1. Ice-sheets height (light blue scale) and land height (brown scale) taken as boundary conditions for the five selected experiments out of twelves. Dark blue-brown limit represents the sea-land mask, and brown-light blue limit represents the land-ice mask.

CPD
11, 27–61, 2015

North American ice sheet influence on the Eurasian climate

P. Beghin et al.

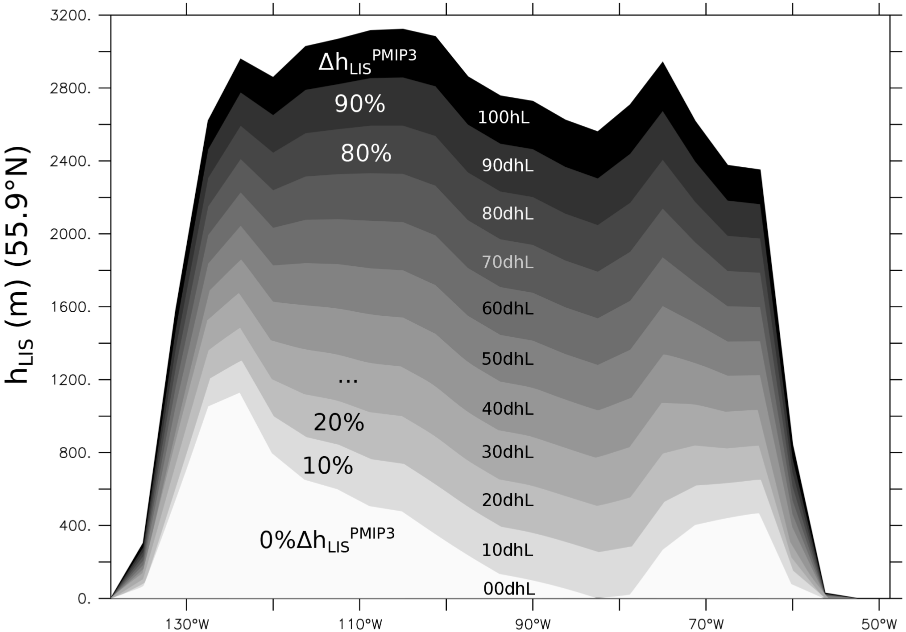

Figure 2. Laurentide ice sheet height depending on the simulation (with name of the corresponding experiment). The height of the LIS depends on the relative difference between PMIP3 Laurentide ice-sheet height and present-day topography ($\Delta h_{\mathrm{PMIP3}}^{\mathrm{LIS}}$).

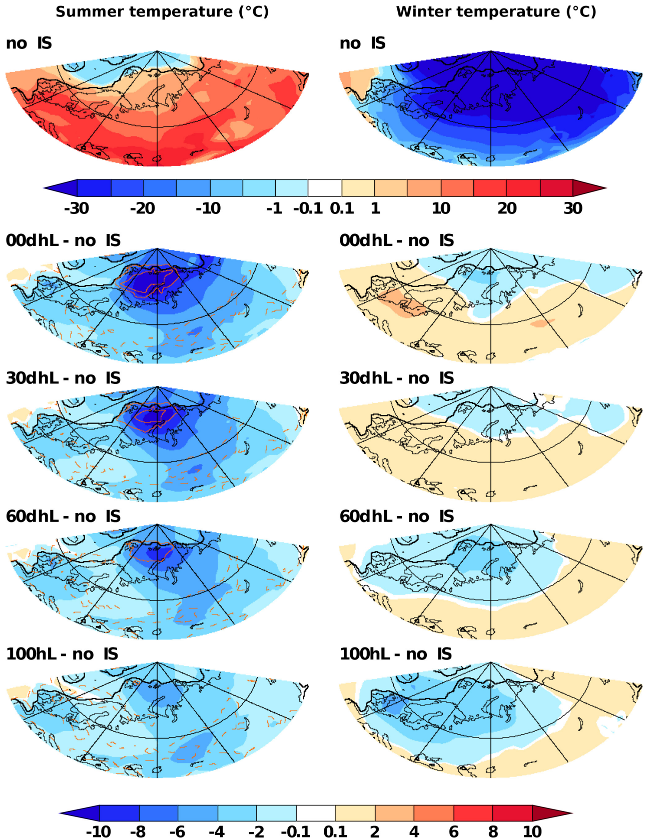

Figure 3. 2 m summer (left) and winter (right) temperature without the LIS (noIS) and anomaly of the 2 m temperature between the *xx* dhL experiment and the noIS experiment: we can therefore quantify the impact of the LIS presence, depending on its topography. Orange contours (left column) are the visible surface albedo difference between *xx* dhL and noIS (contour every 0.2, dashed line is the zero, dotted lines are for negative values).

CPD
11, 27–61, 2015

North American ice sheet influence on the Eurasian climate

P. Beghin et al.

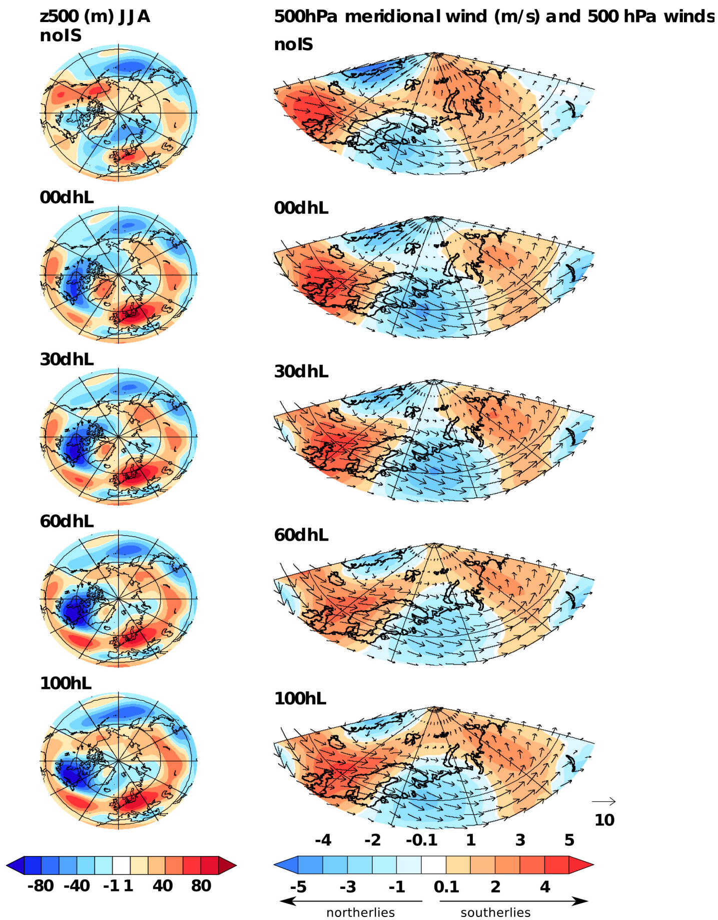

Figure 4. 500 hPa summer geopotential zonal anomaly (left panels) and 500 hPa wind (arrows) and meridional wind (shaded) (right panels).

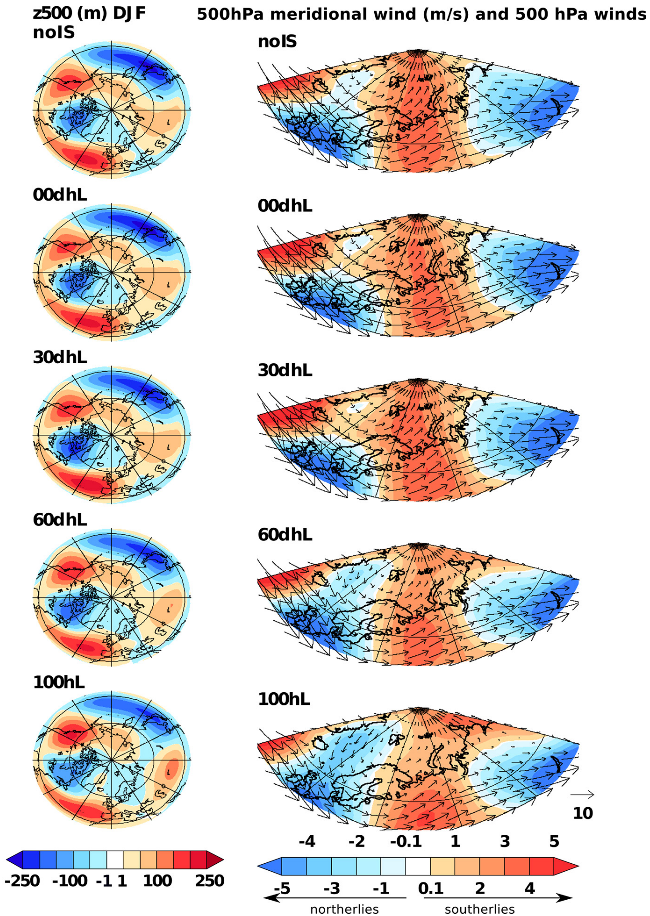

Figure 5. 500 hPa winter geopotential zonal anomaly (left panels) and 500 hPa wind (arrows) and meridional wind (shaded) (right panels).

CPD
11, 27–61, 2015

North American ice sheet influence on the Eurasian climate

P. Beghin et al.

Title Page
Abstract Introduction
Conclusions References
Tables Figures
Back Close
Full Screen / Esc
Printer-friendly Version
Interactive Discussion

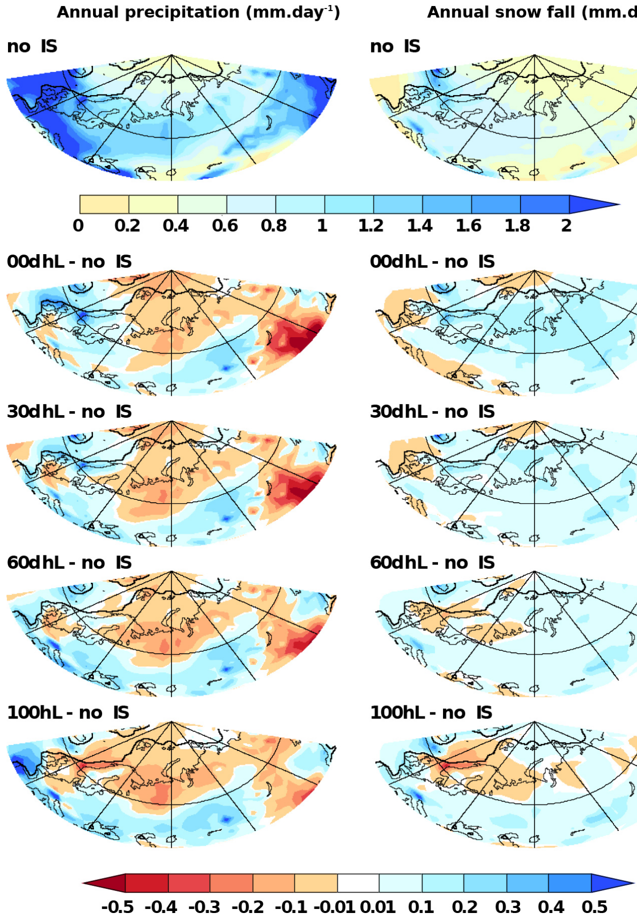

Figure 6. Same as Fig. 3 for annual precipitation (left column) and annual snowfall (right column).

CPD
11, 27–61, 2015

North American ice sheet influence on the Eurasian climate

P. Beghin et al.

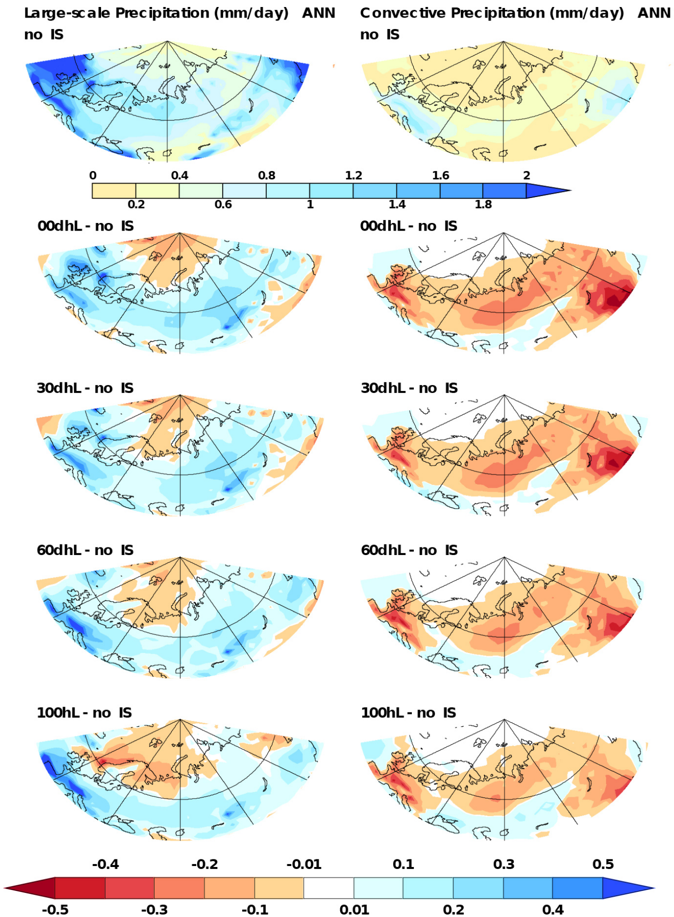

Figure 7. Large-scale (left pannels) and convective (right pannels) annual precipitation without LIS (noLIS experiment), and difference between the *xx* dhL and noLIS experiment of large-scale and convective precipitation.

CPD
11, 27–61, 2015

North American ice sheet influence on the Eurasian climate

P. Beghin et al.

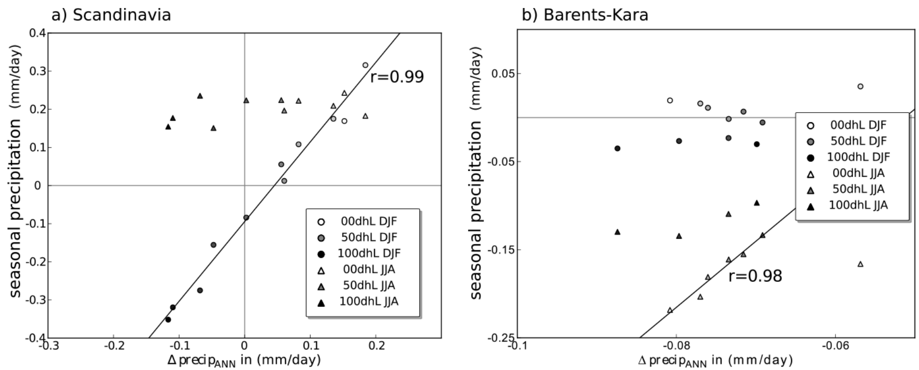

Figure 8. (a) Scandinavian and **(b)** Barents–Kara precipitation anomaly during winter (circles) and summer (triangles) vs. annual precipitation anomaly.

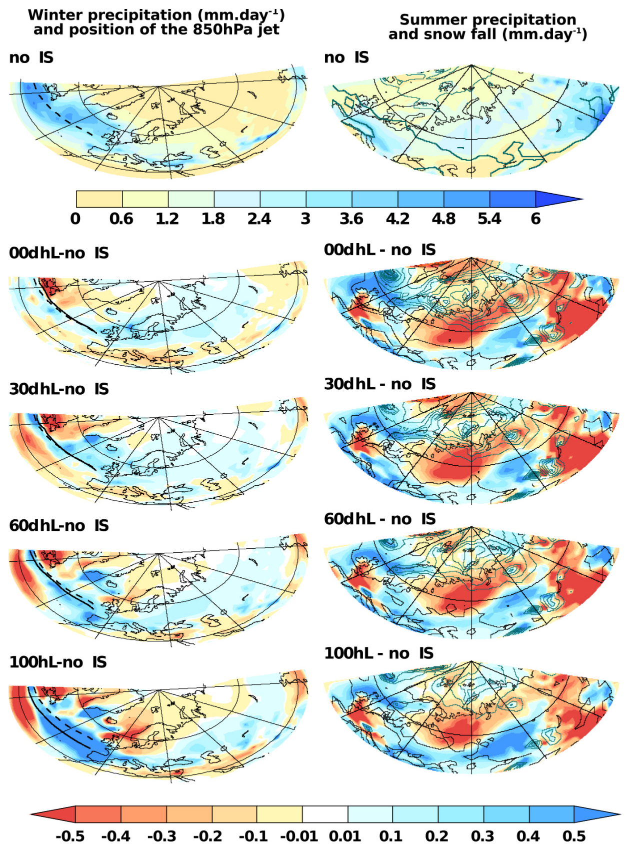

Figure 9. Left column: same as Fig. 3 for winter precipitation (shaded) and position of the Atlantic jet stream without LIS (dashed) and for the corresponding experiment (continuous line). Right column: summer precipitation (shaded) and snowfall (contour every 0.1 mm day^{-1}, blue contour for positive values, orange for negative values).

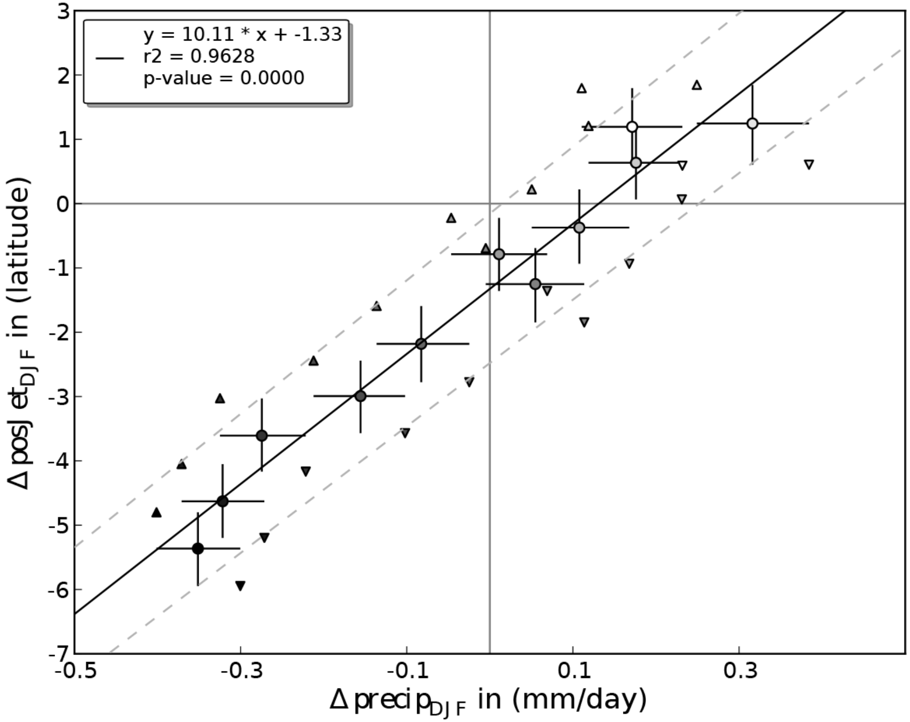

Figure 10. 850 hPa winter jet-stream shift (latitude) versus winter precipitation anomaly over Scandinavian region. Sample of values are obtained by bootstrapping. Triangle up and down represent repectively the 5th precipitation percentile versus the 95th jet position percentile, and the 95th precipitation percentile versus the 5th jet position percentile. Circles are the average and crosses delimited the 5th and 95th percentiles.

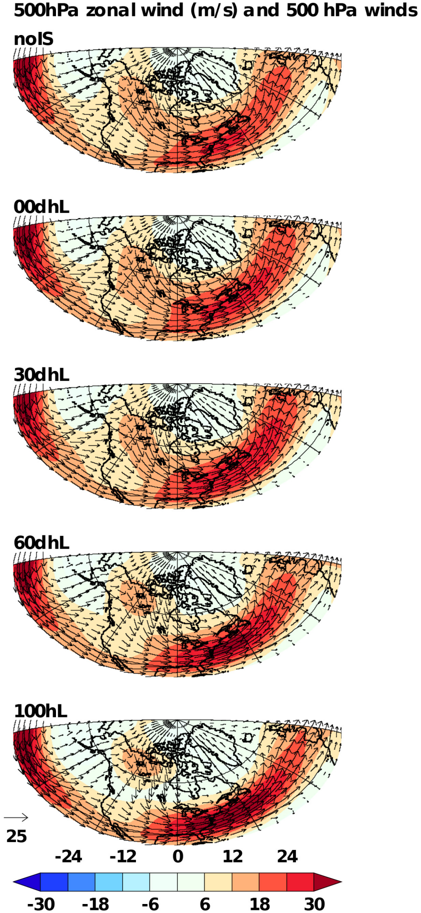

Figure 11. 500 hPa winter wind (arrows) and zonal wind (shaded) in $m\,s^{-1}$.

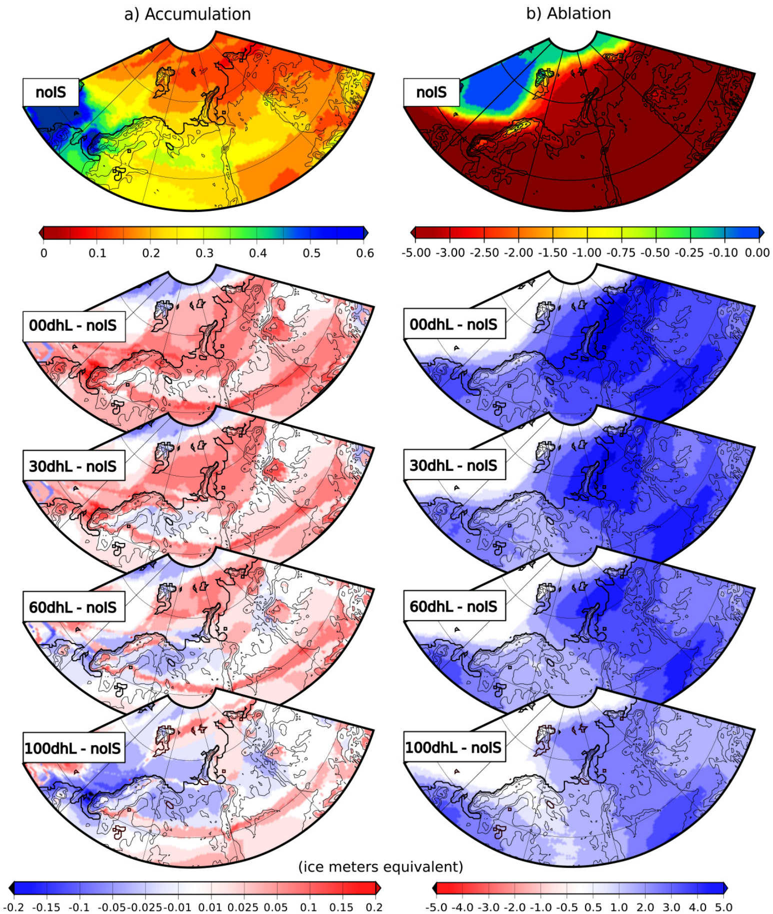

Figure 12. (a) Accumulation computed by the ice-sheet model with the noIS experiment outputs, and anomaly of the accumulation between the *xx* dhL experiment and the noIS experiment. **(b)** Same for the ablation.

CPD
11, 27–61, 2015

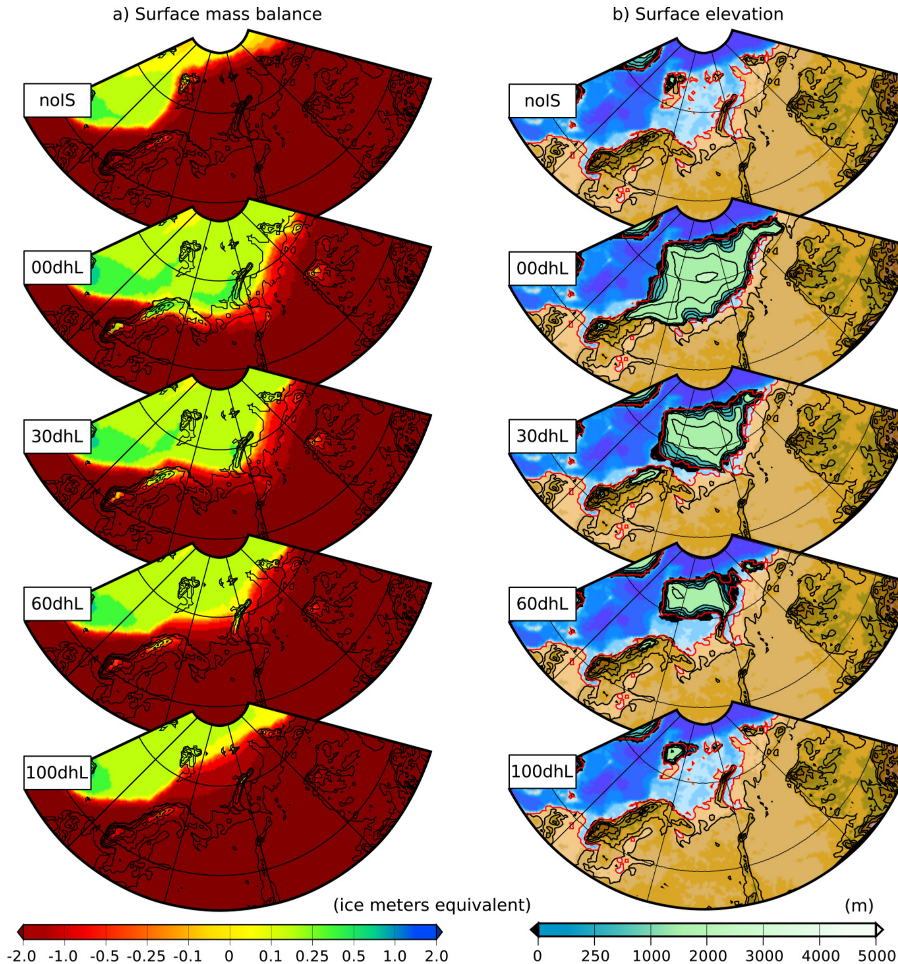

Figure 13. (a) Surface mass balance at the beginning of the simulation and **(b)** surface elevation at the end of the simulation computed by the ice-sheet model for the selected experiments.

CPD
11, 27–61, 2015